IEEE Access
Multidisciplinary | Rapid Review | Open Access Journal

Received March 21, 2021, accepted March 31, 2021, date of publication April 9, 2021, date of current version April 19, 2021.

Digital Object Identifier 10.1109/ACCESS.2021.3072294

Spatially Correlated Dual Hop RIS Aided Next Generation Wireless Systems: An Outage Perspective

RENJITH RAVINDRAN UNNITHAN JALAJA, (Member, IEEE), VETRIVEL CHELIAN THIRUMAVALAVAN, (Graduate Student Member, IEEE), PERIAKARUPAN GURUSAMY SIVABALAN VELMURUGAN, (Member, IEEE), AND SUNDARRAJAN JAYARAMAN THIRUVENGADAM, (Senior Member, IEEE)

Signal Processing Laboratory, Department of Electronics and Communication Engineering, Thiagarajar College of Engineering, Madurai 625015, India

Corresponding author: Vetrivel Chelian Thirumavalavan (vetrivelchelian@student.tce.edu)

ABSTRACT Design and analysis of Reconfigurable Intelligent Surfaces (RIS) assisted new wireless communication systems have attracted much attention among the 6G technology researchers. Recently, studies were made to compare the use of RIS and Decode and Forward (DF) relaying when a weak direct path exists between the transmitter and receiver. Amalgamating the merits of both RIS and DF relay technologies, an RIS assisted DF relay-based cooperative wireless system with energy harvesting is proposed in this paper. A Lambertian model of reflectance is employed in the analysis of the reflecting nature of RIS. Further, the impact of spatial correlation which arises due to the tightly-packed planar RIS array geometry is also considered for performance analysis. By varying inter-element distances and transmit power, the performance of the proposed system is analyzed in terms of outage probability and energy harvesting capability. Numerical expressions are derived for the outage probability of the proposed system and verified using Monte-Carlo simulations. Based on the high performance, the concept of joint use of RIS and DF Relay is extended to the Index Modulation (IM) based wireless system.

INDEX TERMS Energy harvesting, index modulation, outage probability, reconfigurable intelligent surfaces, spatial correlation.

I. INTRODUCTION

Futuristic 6G wireless technologies will supposedly accomplish the expectations not met with 5G. In infrastructure aspect, the key enablers of 6G are envisioned to be Reconfigurable Intelligent Surfaces (RIS), ultra-massive Multiple Input Multiple Output (MIMO) communications, and user-centric networking [1]–[3]. Currently, the research focus is on investigating the customization aspect of the wireless propagation environment [4], [5]. Controllable intelligent channels, enabled by RIS, are utilized to adjust the phase of incident signals such that the signals are added constructively at the end-user. In RIS, arbitrary incident waves are phase tuned by the discrete reflecting elements, and the reflected waves out of RIS, reach the end-user as a coherent wave [6]. In this way, operators can have certain control over the random channel behavior. In [7], it is proved that the RIS aided communications would provide a more favorable path than the free space when the direct link is obstructed. The utilization of RIS for assisting wireless communication has numerous benefits such as facilitation of ultra-reliable link even at very low Signal to Noise Ratio (SNR), low-cost implementation, and energy-efficient hardware. Energy Harvesting (EH) is the enabling factor to improve the energy efficiency in 5G as well as in 6G wireless networks [8]. A realistic power consumption model for RIS based communication is presented in [9]. [10] investigates Simultaneous Wireless Information and Power Transfer (SWIPT) of RIS aided system. It is shown through simulations that RIS aided SWIPT improves the energy efficiency. Wireless energy transfer for RIS aided OFDM system is investigated in [11]. It is shown through theoretical results that it demonstrates ultra energy efficient operation due to RIS assist.

The performance of RIS based communication system is analyzed in detail in [12]. It is also extended to RIS assisted MIMO Index Modulation in [13]. Low power and highly

The associate editor coordinating the review of this manuscript and approving it for publication was Barbara Masini.

secure back-scatter RIS based spatial modulated system is explored in [14]. In [15], hybrid transmitting schemes are proposed for the joint operation of both RIS and Decode and Forward (DF) relaying. Achievable rates of the proposed systems are extensively analyzed and significant performance improvement is observed. In [16], a system model is proposed with two RIS placed side by side to the relay to improve full-duplex performance. A generalized hardware impairment model of RIS aided system is investigated in [17]. When comparing RIS assisted relaying system with conventional MIMO DF relaying system, RIS assisted system has the merit of using only passive elements to aid communication while the latter uses multiple energy-hungry RF chains. Performance between RIS aided communication and relaying are examined in [18]–[21]. All these analysis are based on the assumption of independent and identically distributed (i.i.d) Rayleigh fading channel. However, as the spatial samples at RIS are correlated, the number of independent paths and signal diversity is reduced [22], [23]. Spatial correlation in RIS-aided systems is a very critical factor in analyzing the performance of the systems. An accurate spatial correlation model for RIS systems is presented in [24] as a function of the array geometry of reflecting units. The proposed model in [24] is more accurate than the conventional Kronecker model and in accordance with the 3D Clarke's model [25]. In this paper, the major contributions are summarized as follows:

- A novel co-operative communication system is proposed by combining the merits of RIS and EH in DF relaying system in a Non-Line of Sight (NLOS) wireless environment
- The analytical expressions are derived for the outage performance of the proposed system at both hops, in the presence of spatial correlation at RIS, using the spatial correlation model in [24].
- Alternative approaches are presented to generate correlated Rayleigh envelopes to carry out the outage analysis using simulation.
- Further, the proposed system model is extended with IM at the receiver side. The outage performance of the extended system is also analyzed in the presence of spatial correlation.

A. NOTATIONS

$\lfloor z \rfloor$ denotes the closest integer smaller or equal to z (floor operation). $\mathbb{V}\{z\}$ is the variance of a random variable z. $\mathbb{E}\{z\}$ is the mean of a random variable z. $\mathbb{COV}\{z_1, z_2\}$ is the covariance between random variables z_1 and z_2. $|z|$ denotes the magnitude of a complex random variable z. $\mathcal{N}(\mu, \sigma^2)$ denotes a real Gaussian random variable with mean μ and variance σ^2.

II. SYSTEM MODEL

A three node co-operative wireless communication system is shown in Fig. 1. The proposed RIS-DF-EH system has RIS at both source and destination blocks. RIS at source

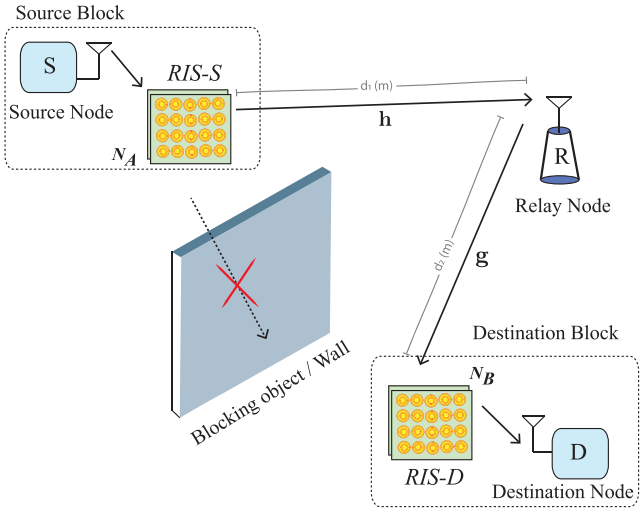

FIGURE 1. The proposed RIS aided DF Relaying System with EH capability (RIS-DF-EH).

block (RIS-S) is located in close proximity to the source node S and is employed as an access point as described in [12, section III]. The advantage of placing RIS in close proximity to the RF source is that the phase compensation is to be performed for the channel between RIS and desired destination only. It is also proved that RIS position must be at either closer to the transmitter or receiver for efficient operation [26], [27]. Similar technique is also used in commercial holographic beamformer [28]. Similarly, RIS at destination block (RIS-D) is placed near the destination node D. The basic motivation of the proposed system is to improve energy harvesting at the relay node for increased operational time and data rate. One of the physical scenarios in which the proposed system can be applied shown in Fig. 2, with Coordinated Multi-Point (CoMP) transmission and reception [29].

Let N_A and N_B be the number of elements of the planar RIS-S and RIS-D respectively. Let $N_A = N_{H_A} \times N_{V_A}$, where N_{H_A} is number of horizontal elements and N_{V_A} is the number of vertical elements in RIS-S. Similarly $N_B = N_{H_B} \times N_{V_B}$. Further, the area of a single RIS reflecting unit is given by $d_{\mathrm{H}} d_{\mathrm{V}}$, where d_{H} and d_{V} are horizontal and vertical inter-element distances respectively. (On the account of RIS reflecting elements being deployed in an edge to edge manner, it is apparent that inter-element distances can be swapped for sides of the reflecting unit).

A plane wave with wavelength λ_c corresponding to the carrier frequency f_c is reflected from RIS-S with the azimuth angle of φ and elevation angle of θ. As the RIS element's surface reflectance behaves as isotropic and diffusely reflecting, the azimuth electromagnetic intensity obeys Lambert's cosine law. The joint Probability Density Function (PDF) of φ and θ is given as

$$f(\varphi, \theta) = \frac{\cos(\theta)}{2\pi}, \quad \varphi \in \left[-\frac{\pi}{2}, \frac{\pi}{2}\right], \theta \in \left[-\frac{\pi}{2}, \frac{\pi}{2}\right] \quad (1)$$

Angular distribution of planar RIS geometry is shown in Fig. 3. It is observed that the resultant scatter plot is

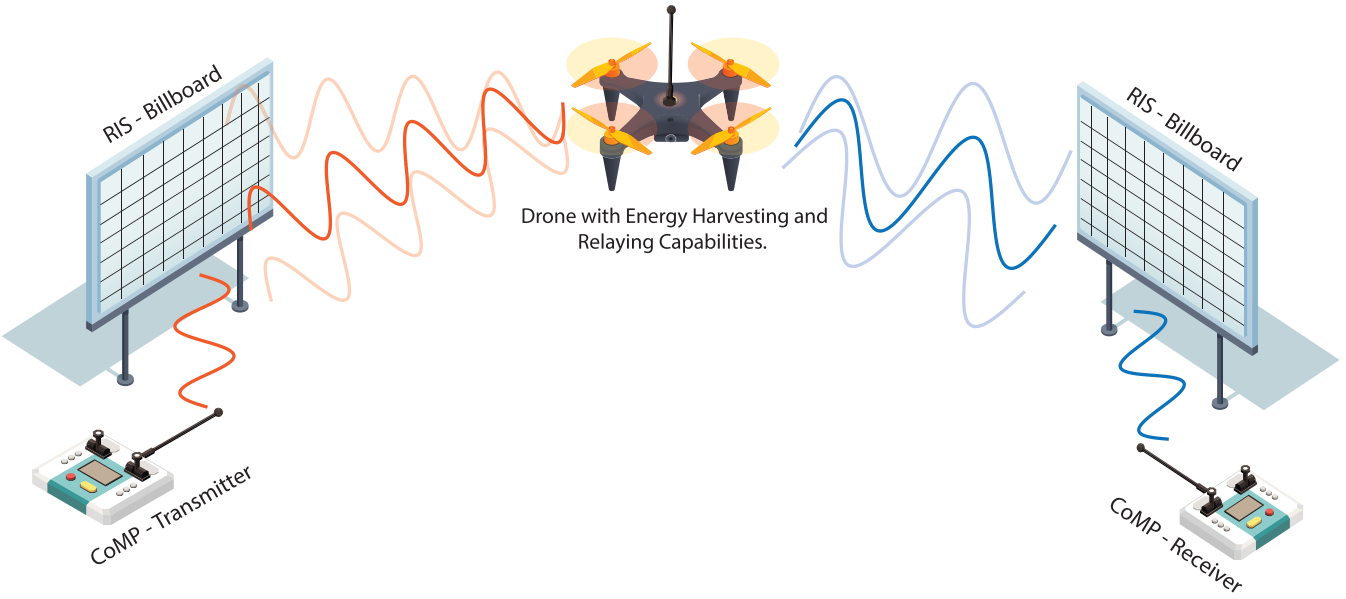

FIGURE 2. Physical Significance of Proposed RIS-DF-EH System.

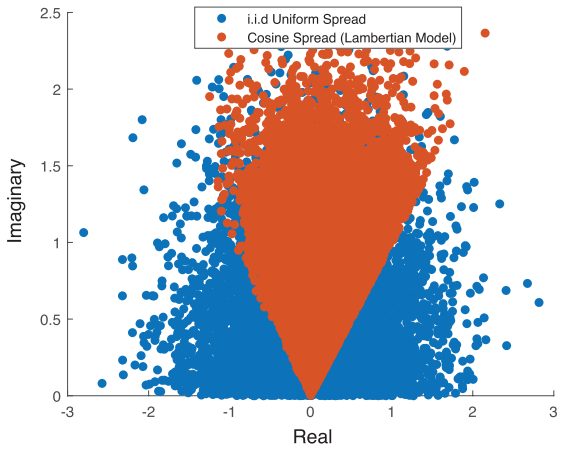

FIGURE 3. Scatter Plots of Planar RIS channel h (using (7)) and i.i.d channel.

highly directional compared to i.i.d. spread. With the angular constraints from (1), the array response vector is given by [24]

$$\mathbf{a}(\varphi,\theta)=\left[e^{\mathrm{j}\mathbf{k}(\varphi,\theta)^{\mathrm{T}}\mathbf{p}_1},\ldots,e^{\mathrm{j}\mathbf{k}(\varphi,\theta)^{\mathrm{T}}\mathbf{p}_{N_A}}\right]^{\mathrm{T}} \tag{2}$$

where $\mathbf{k}(\varphi,\theta)$ is the wavenumber vector. It is defined as

$$\mathbf{k}(\varphi,\theta)=\frac{2\pi}{\lambda_c}\left[\cos(\theta)\cos(\varphi),\ \cos(\theta)\sin(\varphi),\ \sin(\theta)\right]^{\mathrm{T}}. \tag{3}$$

The position vector of the elements in RIS-S is given by

$$\mathbf{p}_n=\left[0,\ \mathrm{mod}\left(n-1,N_{\mathrm{H}_A}\right)d_{\mathrm{H}},\ \left\lfloor(n-1)/N_{\mathrm{H}_A}\right\rfloor d_{\mathrm{V}}\right]^{\mathrm{T}} \tag{4}$$

With isotropic scattering in the half-space in front of the RIS, $(n,m)^{th}$ element of correlation matrix $\mathbf{R_G}=\mathbb{E}\left[\mathbf{a}(\varphi,\theta)\mathbf{a}(\varphi,\theta)^H\right]$ is given by [24, Prop 1]

$$[\mathbf{R_G}]_{n,m}=\mathrm{sinc}\left(\frac{2\|\mathbf{p}_n-\mathbf{p}_m\|}{\lambda_c}\right)\quad n,m=1,\ldots,N_A \tag{5}$$

where $\mathrm{sinc}(x)=\sin(\pi x)/(\pi x)$ is the sinc function.

The covariance matrix ($\mathbf{R_G}$) is defined as

$$\mathbf{R_G}=\begin{pmatrix}1 & \rho_{g1,2} & \rho_{g1,3} & \cdots & \rho_{g1,N_A}\\ \rho_{g2,1} & 1 & \rho_{g2,3} & \cdots & \rho_{g2,N_A}\\ \vdots & & & & \\ \rho_{gN_A,1} & \rho_{gN_A,2} & \rho_{gN_A,3} & \cdots & 1\end{pmatrix} \tag{6}$$

where $\rho_{gi,j}$ are the pairwise covariance values between each complex Gaussian random variables. The real and imaginary part of individual complex Gaussian samples are i.i.d, but the correlation occurs only between the successive pairs of Gaussian random variables.

There are infinitely many multipath components in an isotropic scattering environment between RIS-S and relay node R. By considering L plane waves, the channel between RIS-S and relay node R is modeled as

$$\mathbf{h}=\frac{1}{\sqrt{L}}\sum_{l=1}^{L}c_l\mathbf{a}(\varphi_l,\theta_l) \tag{7}$$

where $c_l\in\mathbb{C}$ is the complex signal attenuation of the lth component, φ_l and θ_l are the azimuth and elevation angles of l^{th} plane wave. The coefficients $c_1,\ldots,c_L$ are i.i.d. with zero mean and variance $d_{\mathrm{H}}d_{\mathrm{V}}$. Using the covariance matrix $\mathbf{R_G}$ from (5), $\mathbf{h}\in\mathcal{N}_{\mathbb{C}}(\mathbf{0},d_{\mathrm{H}}d_{\mathrm{V}}\mathbf{R_G})$. It is noted that channel vector $\mathbf{h}$ is the independently distributed but it is spatially correlated due to RIS geometry. The complex channel coefficient h_i in polar form is represented as $h_i=\alpha_i e^{-j\theta_i}$, α_i is the magnitude of the channel coefficient h_i and modeled as Rayleigh

distributed random variable with $E[\alpha_i] = \sqrt{d_H d_V \pi/4}$ and $\mathbb{V}[\alpha_i] = d_H d_V[4-\pi]/4$.

The relay node R is assumed to be operating in DF mode with EH capability. The M-ary digital modulated RF signal from the source node S is transmitted to the relay node R via RIS-S. Then, the relay node R decodes and re-transmits the signal to the destination node D through RIS-D. Let ϕ_i be the phase shift introduced by the i^{th} reflecting element of the RIS-S. The active phase shifting vector of the RIS-S is defined as $\boldsymbol{\phi} = [\phi_1 \ldots \phi_i \ldots \phi_{N_A}]^T$. The received signal at the relay node R is given by

$$y_R = \sqrt{\frac{P_T}{\beta_{PL1}}}\left[\mathbf{h}^T\boldsymbol{\phi}\right]x + n_R \tag{8}$$

P_T is the transmitted symbol power and large scale channel gain β_{PL1} is a function of propagation distance between RIS-S to R. For the NLOS wireless propagation scenario, β_{PL1} defined as [30, Table 7.4.1-1]

$$\beta_{PL1}(d_1, f_c) = 32.4 + 20\log_{10}(f_c) + 31.9\log_{10}(d_1) - G_t - G_r \tag{9}$$

$1m \leq d_1 \leq 50\, m\, f_c$ defined in GHz. n_R is the received Additive White Gaussian Noise (AWGN) with $\mathcal{N}(0, N_0)$ at the relay node R. G_t and G_r in dB are the antenna gains of source node S and relay node R.

The relay node R is equipped with a power splitter to co-ordinate EH and information processing. More specifically, the power splitting factor λ_{PS} is utilized for EH and $(1-\lambda_{PS})$ for information processing. After energy harvesting, the relay node forwards the decoded symbol to destination node. Hence, from (8) the instantaneous SNR at relay node R during the information processing time is given by,

$$\gamma^R_{inst} = \frac{\left|\mathbf{h}^T\boldsymbol{\phi}\right|^2 P_T\,(1-\lambda_{PS})}{\beta_{PL1}N_0} \tag{10}$$

Considering ideal RIS operation i.e total elimination of the phase component of the channel coefficients at the relay. RIS-S is tuned in a way such that for every $\theta_i + \phi_i = 0\ \forall i$. Let $\left|\sum_{i=1}^{N_A}\alpha_i\right| = \breve{\alpha}$. Then (10) can be written as,

$$\gamma^R_{inst} = \frac{\left|\breve{\alpha}\right|^2 P_T\,(1-\lambda_{PS})}{\beta_{PL1}N_0} \tag{11}$$

$\breve{\alpha}$ is the sum of correlated Rayleigh variables with covariance matrix $\mathbf{R_R}$. Following Central Limit Theorem (CLT), the mean of $\breve{\alpha}$ is expressed as $\mu_{\breve{\alpha}} = N_A\sqrt{d_H d_V \pi/4}$. The convergence is tested and elaborated subsequently. According to CLT, $\breve{\alpha}$ approximates to $\mathcal{N}(\mu_{\breve{\alpha}}, \sigma^2_{\breve{\alpha}})$ for inter-element distances greater than or equal to $0.5\lambda_c$ and for higher values of N_A. This is confirmed by depicting Quantile-Quantile(QQ) plot in Fig. 4 for the inter-element spacing $d_H = d_V = 0.5\lambda_c$. The QQ plot for $d_H = d_V = 0.1\lambda_c$ illustrated in Fig. 5. It is observed that the left tail doesn't follow the standard normal distribution quantile line and it is confirmed that it does not converge to normal distribution.

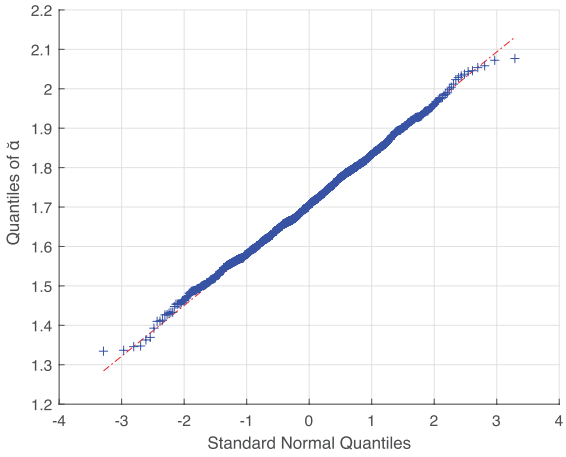

FIGURE 4. QQ Plot of $\breve{\alpha}$ versus Standard Normal for $f_c = 5$GHz, $d_H = d_V = 0.5\lambda_c$.

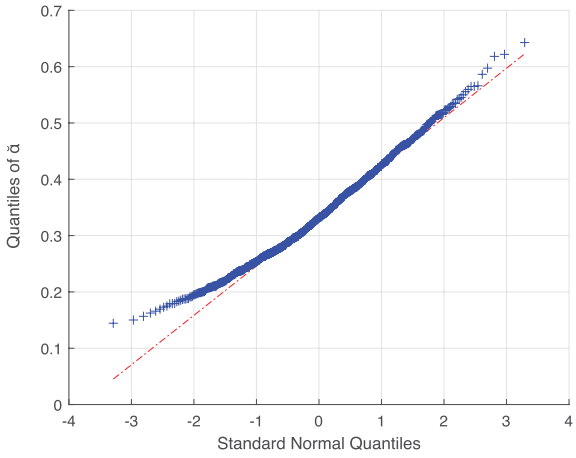

FIGURE 5. QQ Plot of $\breve{\alpha}$ versus Standard Normal for $f_c = 5$GHz, $d_H = d_V = 0.1\lambda_c$ (The CLT convergence does not hold for the correlated case).

As the channel coefficients are spatially correlated, the variance of $\breve{\alpha}$ is determined from $\mathbf{R_R}$. Using [31, (9)], the covariance matrix $\mathbf{R_R}$ is given by

$$\mathbf{R_R} = \sigma_r^2 \mathbf{R_G}^{\circ 2} \tag{12}$$

where σ_r^2 is the variance of a Rayleigh distributed random variable $R = \sqrt{X^2+Y^2}$, where $X \sim \mathcal{N}(0, 0.5)$ and $Y \sim \mathcal{N}(0, 0.5)$, therefore $\sigma_r^2 = \left(\frac{4-\pi}{4}\right)$. $\mathbf{R_G}^{\circ 2}$ denotes Hadamard exponent (elementwise exponent) of $\mathbf{R_G}$ matrix.

Substituting (5) in (12), the elements of covariance matrix ($\mathbf{R_R}$) is defined as

$$[\mathbf{R_R}]_{n,m} = \left(\frac{4-\pi}{4}\right)\mathrm{sinc}^2\left(\frac{2\|\mathbf{p}_n - \mathbf{p}_m\|}{\lambda_c}\right) \tag{13}$$

$n, m = 1, \ldots, N_A$. In a matrix form $\mathbf{R_R}$ is written as

$$\mathbf{R_R} = \sigma_r^2\begin{pmatrix} 1 & \rho^2_{g1,2} & \rho^2_{g1,3} & \cdots & \rho^2_{g1,N_A} \\ \rho^2_{g2,1} & 1 & \rho_{g2,3} & \cdots & \rho^2_{g2,N_A} \\ \vdots & & & & \\ \rho^2_{gN_A,1} & \rho^2_{gN_A,2} & \rho^2_{gN_A,3} & \cdots & 1 \end{pmatrix} \tag{14}$$

Proposition 1: Variance of sum of correlated random variables $(\alpha_1 \ldots \alpha_i \ldots \alpha_{N_A})$ *is the sum of all covariance values of the matrix* $\mathbf{R_R}$.

$$\mathbb{V}(\breve{\alpha}) = \sigma_{\breve{\alpha}}^2 = v^T \left[\mathbf{R_R}\right] v \tag{15}$$

where $v = [1, 1, \ldots 1]^T$ *is the* $N_A \times 1$ *matrix.*

Proof:

$$\mathbb{V}\left(\sum_{i=1}^{n} X_i\right) = \sum_{i=1}^{n} \mathbb{V}\left(X_i\right) + 2 \sum_{1 \le i < j \le n} \mathbb{COV}\left(X_i, X_j\right) \tag{16}$$

Since the covariance matrix $\mathbf{R_R}$ *is square semi-definite and symmetric over its principal diagonal, the trace of the covariance matrix* $\mathbf{R_R}$ *is equal to* $\mathbb{V}\left(X_i\right)$ *and sum of the upper triangular elements is equal to* $\mathbb{COV}\left(X_i, X_j\right)$. *Similarly, the sum of the lower triangular matrix also equals to* $\mathbb{COV}\left(X_i, X_j\right)$. *The overall sum of the elements of the covariance matrix is equal to*

$$\mathbb{V}\left(\sum_{i=1}^{n} X_i\right) = \sum_{i=1}^{n} \sum_{j=1}^{n} \mathbb{COV}\left(X_i, X_j\right) \tag{17}$$

Thus, the variance of sum of correlated random variables $(\alpha_1 \ldots \alpha_i \ldots \alpha_{N_A})$ *can be expressed as*

$$\mathbb{V}(\breve{\alpha}) = \sum_{i=1}^{n} \sum_{j=1}^{n} \rho_{ri,j} \tag{18}$$

In vector form, it is simply written as $\mathbb{V}(\breve{\alpha}) = v^T \left[\mathbf{R_R}\right] v$. ■

Corollary 1: In an ideal isotropic scattering environment, all elements are uncorrelated and $\mathbf{R_G}$ *becomes an identity matrix* $\mathbf{I}$. *Applying CLT,* $\mathcal{N}(\mu_{\breve{\alpha}}, \sigma_{\breve{\alpha}}^2) = \mathcal{N}(N_A\sqrt{d_{\mathrm{H}} d_{\mathrm{V}} \pi/4}, N_A d_{\mathrm{H}} d_{\mathrm{V}}(4-\pi)/4)$. *This case holds only when RIS elements are deployed in a Uniform Linear Array (ULA) geometry with spacing in multiples of half wavelength. In the proposed system, both the RISs are deployed in rectangular array geometry. As the spacings between the diagonal elements are not exact multiples of half wavelength, spatial correlation always exists. The resultant variance is typically lesser than* $tr(\mathbf{R_R}) = N_A d_{\mathrm{H}} d_{\mathrm{V}}(4-\pi)/4$.

Corollary 2: When the elements are fully correlated, $\mathbf{R_G}$ *is equal to ones square matrix. This is practically impossible due to the fact that (5) depends only on inter-element spacing* d_{H} *and* d_{V}. *Ones matrix would essentially mean only one effective element is present. It means that area of the individual RIS element* $A = d_{\mathrm{H}} d_{\mathrm{V}}$ *tends to zero for full correlation. Therefore, the product term* $d_{\mathrm{H}} d_{\mathrm{V}} \mathbf{R_G} \in [\mathbf{0}, \infty \mathbf{R_G}] \approx [\mathbf{0}, \infty \mathbf{I}]$

For notational convenience, let $\breve{\alpha}^2 = A_{\chi^2}$. The PDF of A_{χ^2} is a non-central chi-squared distribution with one degree of freedom and non-centrality parameter $\Lambda_1 = 0.25 d_{\mathrm{H}} d_{\mathrm{V}} N_A \left(\pi(N_A - 1) + 4\right)$. Using $\mathbf{R_R}$ non-centrality parameter Λ_1 is written as [32],

$$\Lambda_1 = (N_A\sqrt{d_{\mathrm{H}} d_{\mathrm{V}} \pi/4})^2 + (v^T \left[\mathbf{R_R}\right] v)$$

In order to represent spatial correlation, it is modified as

$$\Lambda_1 = (N_A\sqrt{d_{\mathrm{H}} d_{\mathrm{V}} \pi/4})^2 + \mathrm{tr}(\mathbf{R_R}) + \sum_{\substack{i=1 \\ i \neq j}}^{N_A} \sum_{j=1}^{N_A} \rho_{ri,j}$$

The last term $\sum_{\substack{i=1 \\ i \neq j}}^{N_A} \sum_{j=1}^{N_A} \rho_{ri,j} = \eta_{sc}$. It represents spatial correlation term. For completely uncorrelated i.i.d, $\eta_{sc} = 0$. Substituting in [33, (1.6)], the PDF of A_{χ^2} is written as

$$\begin{aligned} f_{A_{\chi^2}}(\gamma) &= 0.5 \times exp\left[\frac{-0.5(\gamma + \eta_{sc} + 0.25 d_{\mathrm{H}} d_{\mathrm{V}} N_A \left(\pi(N_A - 1) + 4\right))}{N_0}\right] \\ &\times \left(\frac{\gamma}{\eta_{sc} + 0.25 d_{\mathrm{H}} d_{\mathrm{V}} N_A \left(\pi(N_A - 1) + 4\right)}\right)^{-0.25} \\ &\times I_{-0.5}\left(\sqrt{\eta_{sc} + 0.25 d_{\mathrm{H}} d_{\mathrm{V}} N_A \left(\pi(N_A - 1) + 4\right)\gamma}\right) \end{aligned} \tag{19}$$

III. PERFORMANCE ANALYSIS

A. OUTAGE PROBABILITY AT RELAY ($P_{out}^{R}(\gamma_{th})$)

The outage occurs due to uncertainty of the channel conditions and lower received SNR than the predefined threshold (γ_{th}). Using (11), the outage probability at relay node R is given by,

$$P_{out}^{R}(\gamma_{th}) = \Pr\left[\gamma_{inst}^{R} \le \gamma_{th}\right] = \int_0^{\frac{\gamma_{th}\beta_{PL1} N_0}{P_T(1-\lambda_{PS})}} f_{A_{\chi^2}}(\gamma)\, d\gamma \tag{20}$$

Using [34], the outage probability is expressed as

$$\begin{aligned} P_{out}^{R}(\gamma_{th}) &= 1 - Q_{0.5}\left(\sqrt{\frac{\eta_{sc} + 0.25 d_{\mathrm{H}} d_{\mathrm{V}} N_A \left(\pi(N_A - 1) + 4\right)}{N_0}}, \right. \\ &\left. \sqrt{\frac{\gamma_{th}\beta_{PL1} N_0}{P_T(1-\lambda_{PS})}}\right) \end{aligned} \tag{21}$$

where $Q_M(.,.)$ is the Marcum-Q-function. Using [35], it is expressed as

$$\begin{aligned} P_{out}^{R}(\gamma_{th}) &= -exp\left(-\frac{\eta_{sc} + d_{\mathrm{H}} d_{\mathrm{V}} N_A}{8N_0}\left(\pi(N_A - 1) + 4\right)\right) \\ &\times \left(\frac{d_{\mathrm{H}} d_{\mathrm{V}} N_A}{8N_0}\left(\pi(N_A - 1) + 4\right)\right)\left[\frac{\gamma_l\left(\frac{3}{2}, \frac{\beta_{PL1} N_0}{2P_T(1-\lambda_{PS})}\right)}{\Gamma\left(\frac{3}{2}\right)}\right] \end{aligned} \tag{22}$$

$\gamma_l(.)$ is the lower incomplete gamma function and $\Gamma(.)$ is the upper incomplete gamma function.

B. OUTAGE PROBABILITY AT DESTINATION NODE D ($P_{out}^{D}(\gamma_{th})$)

Time switching policy of energy harvesting and information processing is shown in Fig. 6. ρ is the time proportion for

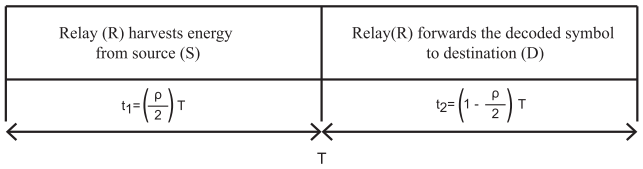

FIGURE 6. TSR protocol at Relay Node for Energy Harvesting and Information Processing.

Time Switching Relay(TSR) protocol and T is the block duration for both EH and information processing. During the time slot $\left(\frac{\rho}{2}\right)T$, the harvested energy at relay node R is given by,

$$E_R = \beta_{PL1}^{-1}\eta\lambda_{PS}P_T d_{\mathrm{H}} d_{\mathrm{V}} A_{\chi^2}\left(\frac{\rho}{2}\right)T \tag{23}$$

where η is the energy efficiency factor. The power available for information transmission at relay node R is given by

$$P_R = \frac{\beta_{PL1}^{-1}\eta\lambda_{PS}P_T d_{\mathrm{H}} d_{\mathrm{V}} A_{\chi^2}\rho}{2\left(1-\frac{\rho}{2}\right)} \tag{24}$$

The received signal at the destination node D is given by,

$$y_D = \sqrt{\frac{P_R}{\beta_{PL2}}}\left[\mathbf{g}^T\boldsymbol{\psi}\right]\hat{x} + n_D \tag{25}$$

$\hat{x}$ is the decoded and re-transmitted symbol from the relay node R. Large scale channel gain β_{PL2} is a function of propagation distance between R to RIS-D. $\mathbf{g} = [g_1, \ldots, g_k, \ldots, g_{N_B}]$, where g_k is the channel coefficient from relay node to the k^{th} reflecting element of RIS-D. $\boldsymbol{\psi_k} = [\psi_1, \ldots, \psi_k, \ldots, \psi_{N_B}]$, ψ_k is the phase shift introduced by the RIS-D. The magnitude component is given by $|g_k| = \beta_k$, also for ideal RIS operation the phase component is nullified i.e $\{\angle g_k\} = 0,\ \forall\, k$ and n_D is the receiver AWGN at destination node. The instantaneous SNR at destination node D is given by

$$\gamma_{inst}^D = \frac{P_R\left|\sum_{k=1}^{N_B}\beta_k\right|^2}{\beta_{PL2}N_0} \tag{26}$$

Let $B_{\chi^2} = \left|\sum_{k=1}^{N_B}\beta_k\right|^2$. B_{χ^2} follows a non-central chi-squared distribution with one degree of freedom and non centrality parameter $\Lambda_2 = \eta_{sc} + 0.25 d_{\mathrm{H}} d_{\mathrm{V}} N_B(\pi(N_B-1)+4)$. Substituting (24) in (26), the instantaneous SNR at destination node is expressed as

$$\gamma_{inst}^D = \frac{\eta\lambda_{PS}P_T\rho A_{\chi^2}B_{\chi^2}}{(2-\rho)\left[\prod_{i=1}^{2}\beta_{PLi}\right]N_0} \tag{27}$$

The outage probability at the destination node D is given by,

$$P_{out}^D(\gamma_{th}) = \Pr\left[\gamma_{inst}^D \le \gamma_{th}\right] \tag{28}$$

Substituting (27) in (28), the outage probability at the destination node P_{out}^D is expressed as,

$$P_{out}^D(\gamma_{th}) = \Pr\left[\frac{\eta\lambda_{PS}P_T\rho A_{\chi^2}B_{\chi^2}}{(2-\rho)\left[\prod_{i=1}^{2}\beta_{PLi}\right]N_0} \le \gamma_{th}\right] \tag{29}$$

Grouping the product of RVs A_{χ^2}, B_{χ^2}, (29) is rewritten as,

$$P_{out}^D(\gamma_{th}) = \Pr\left[A_{\chi^2}B_{\chi^2} \le \frac{\gamma_{th}N_0(2-\rho)\left[\prod_{i=1}^{2}\beta_{PLi}\right]}{\eta\lambda_{PS}P_T\rho}\right] \tag{30}$$

The PDF of the product of two non central chi-square distributions A_{χ^2} and B_{χ^2}, is given by [36], [37]

$$f_{A_{\chi^2}.B_{\chi^2}}(\gamma) = e^{-\frac{1}{2}(\Lambda_1+\Lambda_2)}\sum_{i_1=0}^{\infty}\sum_{i_2=0}^{\infty}\left\{\prod_{h=1}^{2}\frac{\left(\frac{1}{2}\Lambda_h\right)^{i_h}}{i_h!}\right\}\times\{Y\} \tag{31}$$

where

$$Y = \frac{\left(\frac{1}{2}\gamma\right)^{\frac{1}{4}(\kappa_1+\kappa_2)+\frac{1}{2}(i_1+i_2)-1}K_{\frac{1}{2}(\kappa_1-\kappa_2)+i_1-i_2}(\sqrt{\gamma})}{\Gamma\left(\frac{1}{2}\kappa_1+i_1\right)\Gamma\left(\frac{1}{2}\kappa_2+i_2\right)}$$

κ_1 and κ_2 are the degrees of freedom of the A_{χ^2} and B_{χ^2} respectively. $K_g(z)$ is the modified Bessel function of the second kind. The exponentially decaying function is denoted by

$$K_g(z) = \frac{1}{2}\int_0^{\infty} t^{g-1}\exp\left\{-\frac{1}{2}z\left(t+t^{-1}\right)\right\}dt \tag{32}$$

If equal number of reflectors are allocated for source and destination RISs, then $N_A = N_B = N$, $\Lambda_1 = \Lambda_2 = \Lambda$ and $\kappa_1 = \kappa_2 = 1$. The expression for the PDF is simplified as

$$\begin{aligned} &f_{A_{\chi^2}.B_{\chi^2}}(\gamma) \\ &= exp\left(-\eta_{sc} + 0.25 d_{\mathrm{H}} d_{\mathrm{V}} N\left(\pi(N-1)+4\right)\right) \\ &\quad\times\sum_{i_1=0}^{\infty}\sum_{i_2=0}^{\infty}\left(\frac{\frac{1}{2}\left(\eta_{sc}+0.25 d_{\mathrm{H}} d_{\mathrm{V}} N\left(\pi(N-1)+4\right)\right)^{(i_1+i_2)}}{i_1!i_2!}\right) \\ &\quad\times\frac{\left(\frac{1}{2}\gamma\right)^{\frac{1}{2}+\frac{1}{2}(i_1+i_2)-1}K_{i_1-i_2}(\sqrt{\gamma})}{\Gamma\left(\frac{1}{2}+i_1\right)\Gamma\left(\frac{1}{2}+i_2\right)} \end{aligned} \tag{33}$$

The outage probability at destination node D is given by

$$P_{out}^D(\gamma_{th}) = \int_0^{\Upsilon} f_{A_{\chi^2}.B_{\chi^2}}(\gamma)d\gamma \tag{34}$$

where

$$\Upsilon = \frac{\gamma_{th}N_0(2-\rho)}{\eta\lambda_{PS}P_T\rho[\prod_{i=1}^{2}\beta_{PLi}]}$$

A practical approach to solve (49) numerically using simulation software is given in Appendix A.

C. END TO END $P_{out}^{S\to D}$

An outage occurs if the end-to-end SNR of any link i.e.,$\gamma_{S\to R}$ or $\gamma_{R\to D}$ falls below an outage threshold γ_{th}. The overall outage probability at the destination node $P_{out}^{S\to D}(\gamma_{th})$ is written as,

$$P_{out}^{S\to D}(\gamma_{th}) = P_{out}^{R} + \left[\left(1 - P_{out}^{R}\right) \times P_{out}^{D}\right] \tag{35}$$

IV. RIS AIDED DF RELAYING INDEX MODULATED SYSTEM WITH EH (RIS-DF-IM-EH)

In this section, RIS Aided DF Relaying Index Modulated System with EH (RIS-DF-IM-EH) is proposed as an extension to improve the spectral efficiency of the proposed system in section III. In conventional Index Modulation (IM) system, the indices of transmit antenna are used to provide additional information along with an M-ary modulated carrier to increase spectral efficiency [38], [39]. The proposed IM system is inspired from RIS-IM scheme involving receive antenna index to transmit additional spatial bits as proposed in [13, Section II-B]. The system model is shown in Fig. 7. One of the physical scenarios in which the proposed IM-DF-RIS relay system can be applied is shown in Fig. 8 with CoMP transmission and reception.

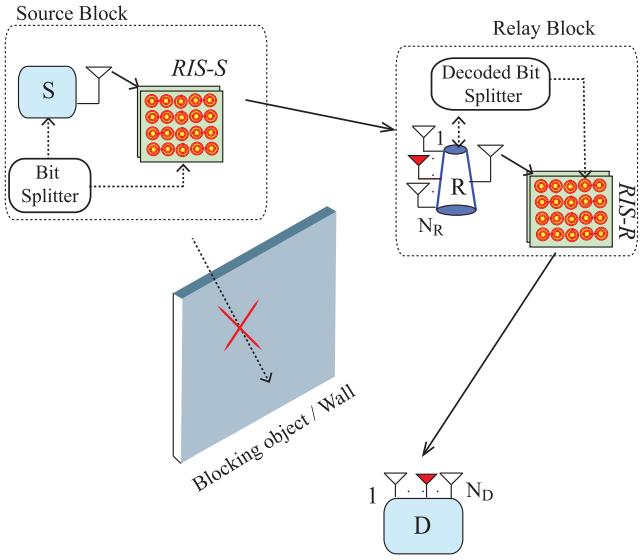

FIGURE 7. The proposed RIS Aided DF Relaying Index Modulated System with EH capability (RIS-DF-IM-EH).

In the first hop of the proposed RIS-DF-IM-EH, the information bits from the source node S are clustered into two groups $log_2\ N_R$ (Spatial bits) and $log_2\ M$ (Data bits). M denotes to the number of digital modulation symbols per transmission. The first group of $log_2\ N_R$ adjusts the RIS-S phases according to the selected receive antenna at relay node R with index p.

The spatial bits are sent to RIS-S controller system via the bit-splitter and the reflection parameters are appropriately changed such that the signal reaches the desired antenna at relay node R. The second group of $log_2\ M$ is transmitted using single RF chain from source node S.

The received signal at the p^{th} receive antenna of the relay node is written as

$$y_{Rp} = \sqrt{P_S}\left[\sum_{i=1}^{N_A} h_{p,i}e^{j\phi_i}\right]x + n_R, \quad p \in \{1, \ldots, N_R\} \tag{36}$$

$h_{p,i}$ is the channel coefficient from i^{th} reflecting element of RIS-S to the p^{th} receive antenna at the relay node. The complex channel coefficient in polar form is, $h_i = \alpha_i e^{-j\theta_i}$, α_i is the magnitude (real) component of the channel coefficient h_i with Rayleigh distribution with $\mathbb{E}[\alpha] = \sqrt{d_H d_V \frac{\pi}{4}}$ and $\mathbb{V}[\alpha] = \frac{d_H d_V[4-\pi]}{4}$. ϕ_i is the phase shift introduced by the i^{th} reflecting element of the RIS-S, x is the transmitted symbol and n_R is the received AWGN with $\mathcal{N}(0, N_0)$ at the relay node. Similarly to the previous case, the relay is equipped with a power splitter to co-ordinate EH and information processing. More specifically, the power splitting factor λ_{PS} is utilized for EH and $(1-\lambda_{PS})$ for information processing. For further clarity, Maximum Likelihood (ML) detection for the proposed RIS-DF-IM-EH operation involves joint decoding of both antenna index p and the symbol x at relay node R is given as

$$(\hat{p}, \hat{x}) = \arg\min_{(p,x)} \sum_{p=1}^{N_R} \left| y_{Rp} - \sqrt{P_S}\left[\sum_{i=1}^{N_A} h_{p,i}e^{j\phi_i}\right]x \right|^2 \tag{37}$$

From (36), instantaneous SNR at the RIS-DF-IM-EH relay node R is given by

$$\gamma_{inst\{IM\}}^{R} = \frac{\left|\sum_{i=1}^{N_A} h_{\hat{p},i}e^{j\phi_i}\right|^2 P_T \beta_{PL1}\,(1-\lambda_{PS})}{N_0} \tag{38}$$

$\hat{p}$ denotes the selected antenna index.

A. OUTAGE PROBABILITY AT RELAY ($P_{out}^{R}(\gamma_{th})$)

The index modulated channel between the source nodes and relay node R consists of N_R independent paths. Ideal operation of RIS-S is considered to eliminate all the phase components of the channel. Hence, the PDF of the IM channel is modeled by substituting $\kappa = N_R$ degrees of freedom in the PDF from (19) of non-central chi-squared distribution for IM case is given as,

$$\begin{aligned} f_{A_{\chi^2}}^{IM}(\gamma) &= \frac{1}{2} exp\left[-0.5(\gamma + \eta_{sc} + 0.25 d_H d_V N_A\,(\pi(N_A-1)+4))\right] \\ &\times \left(\frac{\gamma}{(\eta_{sc} + 0.25 d_H d_V N_A\,(\pi(N_A-1)+4))}\right)^{\frac{N_R}{4}-\frac{1}{2}} \\ &\times I_{N_R/2-1}\left(\sqrt{(\gamma\,\eta_{sc} + 0.25 d_H d_V N_A\,(\pi(N_A-1)+4))}\right) \end{aligned} \tag{39}$$

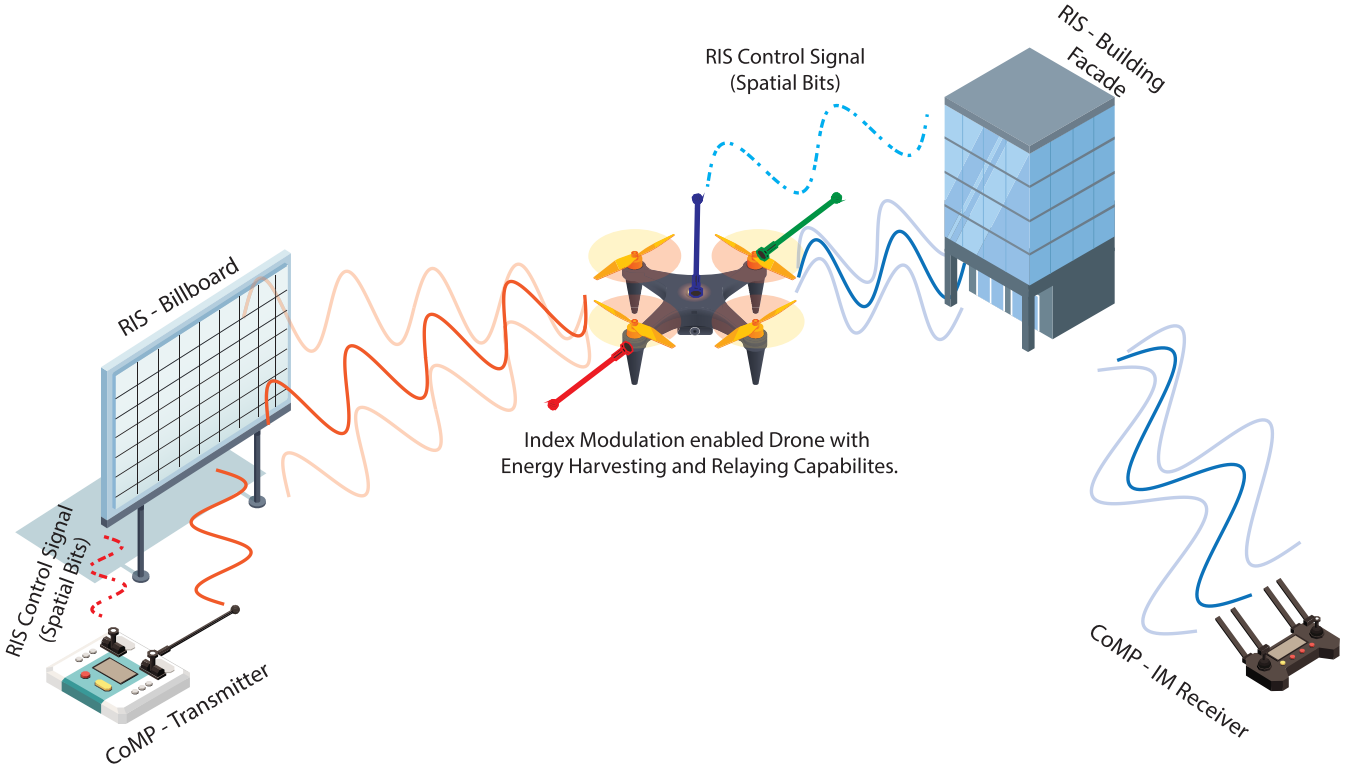

FIGURE 8. Physical Significance of RIS-DF-IM-EH System.

where

$$I_{N_R/2-1}(\sqrt{\Lambda\gamma}) = \left(\sqrt{(\gamma\eta_{sc} + 0.25 d_{\mathrm{H}} d_{\mathrm{V}} N_A\,(\pi(N_A-1)+4))/2}\right)^{\frac{N_R}{2}-1} \times \sum_{j=0}^{\infty} \frac{((\gamma\eta_{sc} + 0.25 d_{\mathrm{H}} d_{\mathrm{V}} N_A\,(\pi(N_A-1)+4))/4)^j}{j!\Gamma(N_R/2+j)} \tag{40}$$

The probability of outage at the RIS-DF-IM-EH relay node is given by the $P^R_{out}(\gamma_{th}) = \Pr\left[\gamma^R_{inst} \le \gamma_{th}\right]$. It is determined as

$$P^R_{out}(\gamma_{th}) = 1 - Q_{N_R/2}\left(\sqrt{\frac{N}{4}(N\pi+4-\pi)}, \sqrt{\left(\frac{\gamma_{th}\beta_{PL1}N_0}{P_T(1-\lambda_{PS})}\right)}\right) \tag{41}$$

B. OUTAGE PROBABILITY AT DESTINATION NODE D

In the second hop of the proposed RIS-DF-EH-IM, the relay node R forwards the decoded bits both spatial and data bits to the destination node D using the harvested energy. Similar to the first hop, the first group of $log_2\ N_D$ adjusts the RIS-R phases according to the selected receive antenna at destination node D with index q. The spatial bits are sent to RIS-R controller system via the bit-splitter and the reflection parameters are appropriately changed such that the signal reaches the desired antenna at destination node D. The second group of $log_2\ M$ is transmitted using single RF chain from relay node R.

RIS-DF-IM-EH relay node R harvests energy and then re-transmits the signal to destination with the aid of decoded bit splitter to tune the RIS-R. Single transmit antenna at relay node R is used in transmission of the modulated signal to the RIS-R elements placed in the near proximity of the relay node R (similar to Wireless Access Point (WAP) operation) [12], [13]. RIS-R reflects the beam to the desired destination antenna index q. The received signal at destination node D is given by

$$y_{Dq} = \sqrt{P^{IM}_R}\left[\sum_{i=1}^{N_B} g_{q,i} e^{j\psi_i}\right] x + n_D \tag{42}$$

$q \in \{1, \ldots, N_D\}$

The instantaneous SNR at the destination node D is expressed as

$$\gamma^D_{inst\{IM\}} = \frac{P^{IM}_R \left|\sum_{k=1}^{N_B} \beta_k\right|^2}{N_0} \tag{43}$$

As described in previous section, substituting (24) in (43) the instantaneous SNR is written as

$$\gamma^D_{inst\{IM\}} = \frac{\eta\lambda_{PS} P_T \beta_{PL1}\beta_{PL2}\rho A^p_{\chi^2} B^q_{\chi^2}}{(2-\rho)N_0} \tag{44}$$

where $A^p_{\chi^2} = \left|\sum_{i=1}^{N_A} \alpha_i\right|^2$ and $B^q_{\chi^2} = \left|\sum_{i=1}^{N_B} \beta_i\right|^2$. Both $A^p_{\chi^2}$ and $B^q_{\chi^2}$ are non-central chi-squared distribution with degrees

of freedom N_R and N_D and non-centrality parameters Λ_1 and Λ_2 respectively. The PDF of the product of $A^p_{\chi^2}B^q_{\chi^2}$,

$$f^{IM}_{A^p_{\chi^2}.B^q_{\chi^2}}(\gamma) = e^{-\frac{1}{2}(\Lambda_1+\Lambda_2)} \sum_{i_1=0}^{\infty}\sum_{i_2=0}^{\infty}\left\{\prod_{h=1}^{2}\frac{\left(\frac{1}{2}\Lambda_h\right)^{i_h}}{i_h!}\right\} \times \frac{\left(\frac{1}{2}\gamma\right)^{\frac{1}{4}(N_R+N_D)+\frac{1}{2}(i_1+i_2)-1} K_{\frac{1}{2}(N_R-N_D)+i_1-i_2}(\sqrt{\gamma})}{\Gamma\left(\frac{1}{2}N_R+i_1\right)\Gamma\left(\frac{1}{2}N_D+i_2\right)} \tag{45}$$

From (45), the probability of outage P^D_{out} at destination node D is written as

$$P^D_{out}(\gamma_{th}) = \int_0^{\frac{\gamma_{th}N_0(2-\rho)}{P_T\beta_{PL1}\eta\rho\lambda_{PS}}} f^{IM}_{A_{\chi^2}.B_{\chi^2}}(\gamma)d\gamma \tag{46}$$

V. RESULTS AND DISCUSSIONS

In this section, the performance of the proposed systems is analyzed using derived analytical expressions and simulations parameters listed in Table 1. It is assumed that $d_{\mathrm{H}} = d_{\mathrm{V}}$ and same at both RIS-S and RIS-D. Using (5), the variations in spatial correlation between the first and second elements are shown in Fig. 9 with respect to the change in inter-element spacing. For simulation purpose, two algorithms are given in Appendix B to generate correlated Rayleigh envelopes. It is observed that both the algorithms exhibit perfect match between the theoretical and simulation values of spatial correlation. It is also verified using numerical integration of $\mathbb{E}\left[\boldsymbol{a}(\varphi,\theta)\boldsymbol{a}(\varphi,\theta)^H\right]$ [24, (9)]. The noise variance N_0 in dBm is modeled through [40]

$$N_0 = -174 + 10\log_{10}(\mathrm{B[Hz]}) - \mathrm{SNR[dB]} \tag{47}$$

and P_T is assumed to be unity.

The outage performance of the proposed system at the relay node R is shown in Fig. 10 with respect to SNR (in dB) and spatial correlation coefficients. It is inferred that outage probability increases as spatial correlation increases since it introduces severe degradation in signal diversity. The outage performance at the relay node R of the proposed RIS-DF-EH system is shown in Fig. 11 with respect to SNR (in dB) and inter-element distances. From the color map plot, it is inferred that simultaneous increase in SNR and the inter-element

TABLE 1. Simulation Parameters.

Simulation Parameters	Values
$N = N_A = N_B$	64 (8X8) Planar Array $d_{\mathrm{H}} = d_{\mathrm{V}}$
f_c	5GHz
λ_{PS}	0.5
ρ	0.5
η	1
Target data rate	10 bits/s/Hz
G_t	5 dB
G_r	5 dB
d_1	10 m
d_2	10 m

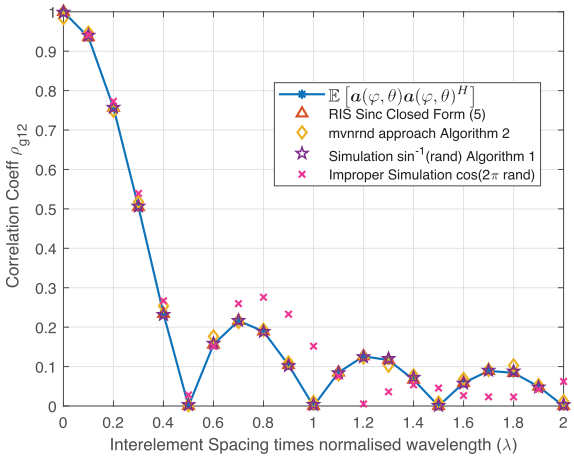

FIGURE 9. Spatial Correlation Coefficient $\rho_{g1,2}$ as a function of Inter-element spacing.

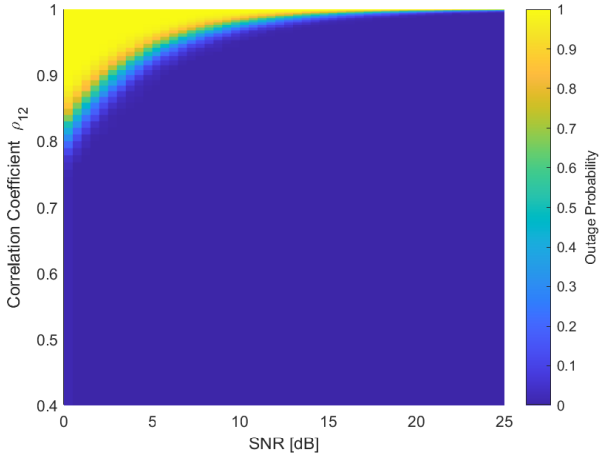

FIGURE 10. Outage Performance of 8 × 8 RIS-DF-EH Relay Node as a function of Correlation Coefficient $\rho_{g1,2}$. ($\lambda_{PS} = 0.5$, $d_1 = 10$ m, $f_c = 5$GHz).

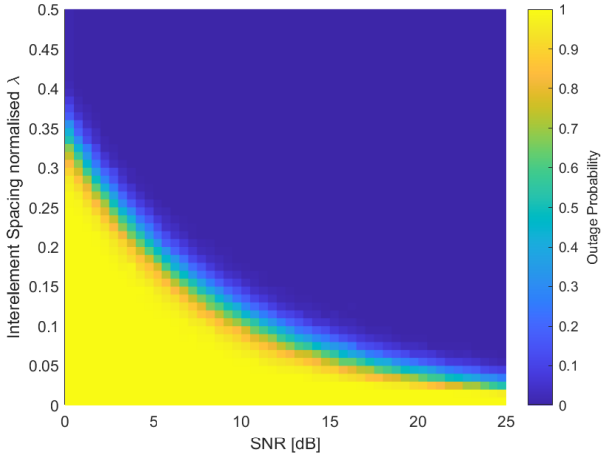

FIGURE 11. Outage Performance of 8 × 8 RIS-DF-EH Relay Node as a function of Inter-element Spacing $\rho_{g1,2}$. ($\lambda_{PS} = 0.5$, $d_1 = 10$ m, $f_c = 5$GHz).

spacing substantially improves the outage performance of the proposed system. The dark blue quadrant refers to no outage zone, i.e., the capacity exceeds the threshold of 10 bits/s/Hz and the yellow area in the bottom left depicts a full outage region. As expected, tight packing (high spatial correlation) and low SNR level cause severe degradation in outage performance. The ergodic capacity at the relay node R is shown in Fig. 12. A maximum of 19.6 bits/s/Hz is achieved at 25dB with $d_{\mathrm{H}} = d_{\mathrm{V}} = 0.7\lambda_c$.

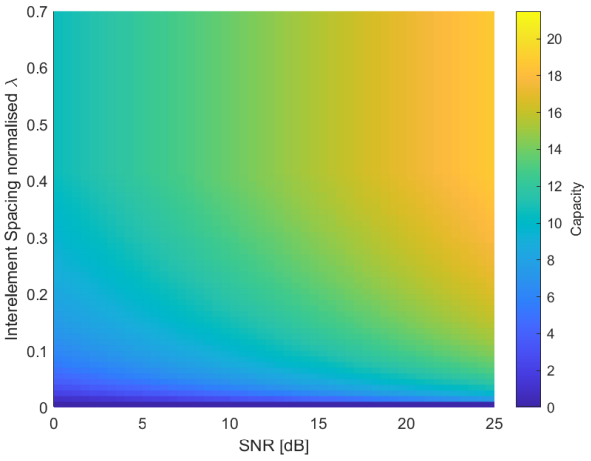

FIGURE 12. Capacity of 8 × 8 RIS-DF-EH Relay Node as a function of Inter-element Spacing $\rho_{g1,2}$. ($\lambda_{PS} = 0.5$, $d_1 = 10$ m, $f_c = 5$GHz).

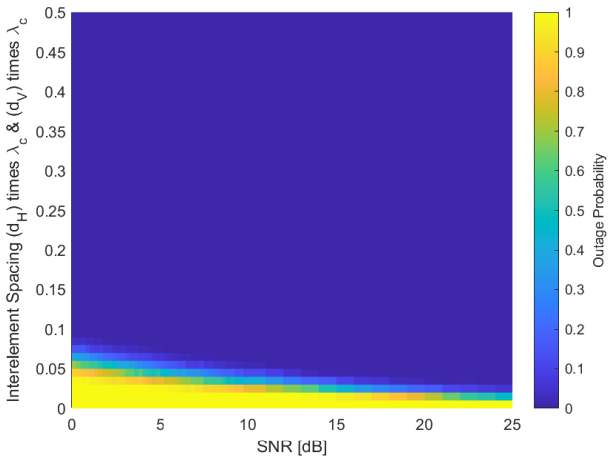

FIGURE 13. Outage Performance of 8 × 8 RIS-DF-EH at the Destination Node as a function of Inter-element Spacing $\rho_{g1,2}$. ($\lambda_{PS} = 0.5$, $d_1 = 10$ m, $f_c = 5$GHz).

The outage performance and ergodic capacity at the destination node of the proposed system are shown in Fig. 13 and Fig. 14 with respect to SNR (in dB) and inter-element distances. The maximum capacity is around 30 bits/s/Hz at 25dB SNR and 0.7 inter-element distance. This due to fact that the signal experiences two independent RIS phasing operations. The energy harvesting capability of the proposed systems is shown in Fig. 16. When the power splitting factor

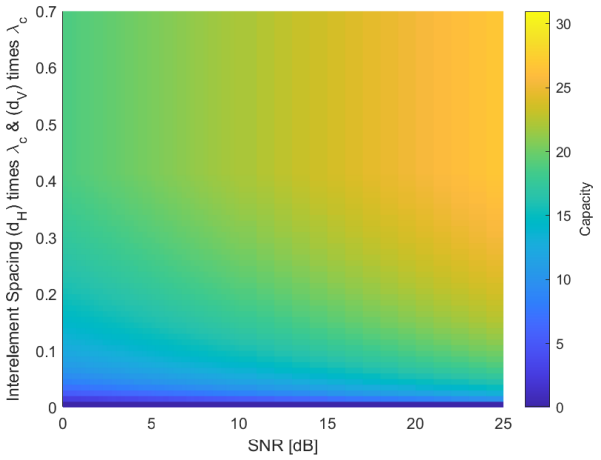

FIGURE 14. Capacity of 8 × 8 RIS-DF-EH at the Destination Node as a function of Inter-element Spacing ($\lambda_{PS} = 0.5$, $d_1 = 10$ m, $f_c = 5$GHz).

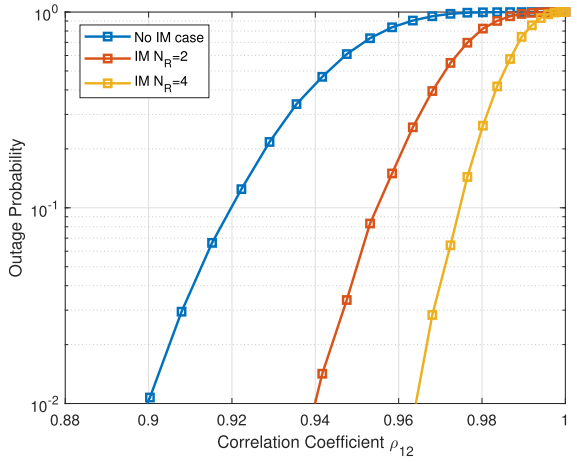

FIGURE 15. Outage Performance at Relay Node for RIS-DF-EH and IM cases. ($SNR = 5dB$ $\lambda_{PS} = 0.5$, $d_1 = 10$ m, $f_c = 5$GHz).

and $d_{\mathrm{H}} = d_{\mathrm{V}}$ are increased, the average harvested energy is also increased (23).

Using Fig. 15, the relationship between the correlation coefficient and outage probability is analyzed for three different cases: i) without IM, ii) IM with $N_R = 2$ and iii) IM with $N_R = 4$. It is inferred that in 'without IM' the outage probability of 10^{-1} is at correlation coefficient 0.92, whereas in 'IM with $N_R = 2$' and IM with $N_R = 4$, outage probability of 10^{-1} is at correlation coefficient 0.95 and 0.97 respectively. As expected, IM improves the degrees of freedom and provides enhancement in maximum capacity of the RIS-DF-EH systems by the excess sum of $log_2(N_R)$.

The harvested energy at relay node R, as a function of SNR is shown in Fig 17, with 8 × 8 square geometry RIS, $d_{\mathrm{H}} = d_{\mathrm{V}} = 0.5\ \lambda$ and $d_1 = 10$m and carrier frequency 5 GHz. The EH capability is analysed in the following three cases:

1) With RIS and perfect compensation of phase distortion introduced by the channel. Harvested energy is calculated using (23).

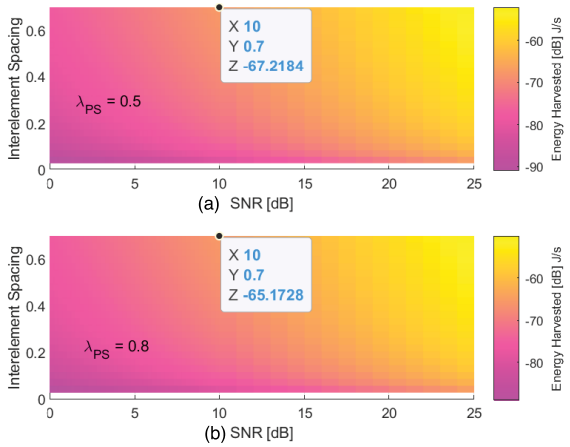

FIGURE 16. Energy harvested per unit time in J/s for 8 × 8 RIS system at Relay Node) ((a) $\lambda_{PS} = 0.5$ and (b) 0.8, $d_1 = 10$ m, $f_c = 5$GHz).

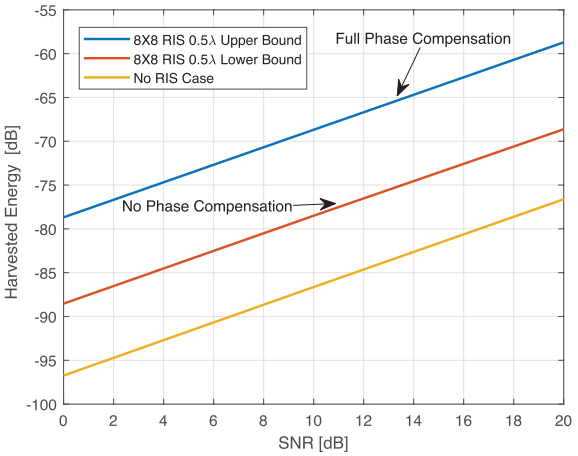

FIGURE 17. Energy harvested per unit time in J/s for 8 × 8 RIS system at Relay Node. ($\lambda_{PS} = 0.5$, $d_1 = 10$ m, $f_c = 5$GHz).

2) With RIS and no compensation for phase distortion. Only aperture gain ($Nd_{\mathrm{H}}d_{\mathrm{V}}$) is obtained in this case.
3) Without the use of RIS in the system.

It is observed that the harvested energy in case 1 is approximately 20dB more than the system without RIS.

VI. CONCLUSION

In this paper, the impact of spatial correlation among RIS elements in a rectangular array geometry is analyzed. A numerical approach for evaluating the product of two non-central chi-squared distribution is established as well. A novel co-operative RIS aided DF relaying with EH is proposed. The proposed system can enhance received signal power using constructive channel path utilization. Also, a substantial improvement is observed in harvested energy at the relay node. The proposed system model is extended to IM schemes for further improvement in outage performance. Both the theoretical and simulation results have perfect matching even at low SNRs and high spatial correlation. With the aforementioned characteristics, it is noted that the proposed systems provide a realistic analysis of the impact of spatial correlation on the tightly packed RIS array geometry.

APPENDIX-A

The joint PDF of

$$\begin{aligned} &f_{A_{\chi^2}.B_{\chi^2}}(\gamma) \\ &= exp\left(-\eta_{sc} + 0.25 d_{\mathrm{H}} d_{\mathrm{V}} N\left(\pi(N-1)+4\right)\right) \\ &\times \sum_{i_1=0}^{\infty}\sum_{i_2=0}^{\infty}\left(\frac{\frac{1}{2}\left(\eta_{sc}+0.25 d_{\mathrm{H}} d_{\mathrm{V}} N\left(\pi(N-1)+4\right)\right)^{(i_1+i_2)}}{i_1! i_2!}\right) \\ &\times \frac{\left(\frac{1}{2}\gamma\right)^{\frac{1}{2}+\frac{1}{2}(i_1+i_2)-1} K_{i_1-i_2}(\sqrt{\gamma})}{\Gamma\left(\frac{1}{2}+i_1\right)\Gamma\left(\frac{1}{2}+i_2\right)} \end{aligned} \tag{48}$$

The outage probability at destination node D is given by

$$P_{out}^{D}(\gamma_{th}) = \int_0^{\Upsilon} f_{A_{\chi^2}.B_{\chi^2}}(\gamma) d\gamma \tag{49}$$

where

$$\Upsilon = \frac{\gamma_{th} N_0 (2-\rho)}{\eta \lambda_{PS} P_T \rho [\prod_{i=1}^{2} \beta_{PLi}]}$$

It describes a finite integral numerical solution for the probability of outage at destination P_{out}^{D}. Closed-form solution using Maclaurin approximations is not possible as it has a modified Bessel function of second kind. When $\gamma \to 0$ then $K_g(\sqrt{\gamma}) \to \infty$ and the exponentially decaying term inside the equation. In numerical computing environment such as MATLAB ®, overloading it with twin infinite series is not recommended. Instead, an asymptotically equivalent finite sum solution for the nested infinite series in (49) is essential. The higher bound for i_{1max} increases the upper bound of the solution to the integral higher than unity and conversely higher bound for i_{2max} decreases the solution to very low values. In a numerical computation, the minimum value of upper limits of i_1 and i_2 are found by solving the following

$$\int_0^{\Upsilon} \sum_{i_1=0}^{i_1 max}\sum_{i_2=0}^{i_2 max} f_{A_{\chi^2}.B_{\chi^2}}(\gamma) d\gamma = \begin{cases} 1 & \text{if } \dfrac{P_T}{N_0} \to -\infty dB \\ 0 & \text{if } \dfrac{P_T}{N_0} \to +\infty dB \end{cases}$$

The outage probability at the destination node D is shown in Fig. 18 with $d_{\mathrm{H}} = d_{\mathrm{V}} = 0.5\lambda_c$. It is observed that there is a tight match between the theoretical and simulation results.

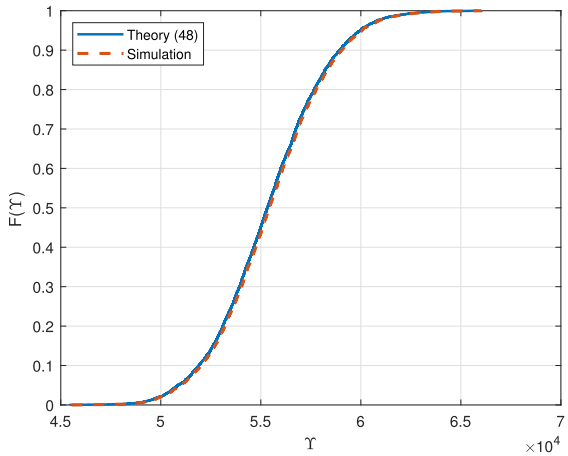

FIGURE 18. Verification of theory in (48) and simulation through CDF.

APPENDIX-B

Algorithm 1 Algorithm for Generating Correlated Rayleigh Envelopes for the Given RIS Array Geometry

Input: $\lambda, d_H, d_V, N_H, N_V$, mc-iteration
Output: $\mathbf{h}, P_{out}$
Initialization:
Phiall is a evenly spaced vector $[-\pi/2, \pi/2]$ with N_c points.
Obtain $\mathbf{pos}_n \in \mathbb{R}^{3XN}$
Monte Carlo
for mc = 1 to 1000 **do**
  for Npath = 1 to 100 **do**
    $\theta = sin^{-1}$(RAND)
    ϕ = Phiall(RANDI(y))
    Generate $k(\theta, \phi)$ vector
    Compute array response $a(\theta, \phi)$ vector through $k(\theta, \phi)$ and $\mathbf{pos}_n$
    $\mathbf{h}$ = multiply $a(\theta, \phi)$ by i.i.d $\mathcal{CN}$
  end for
end for
return h

Note: RAND is uniformly generated random variable ($0 \leq x \leq 1$). RANDI(u) is uniformly distributed random variable ($0 \leq u \leq N_c$). Properly simulating cosine PDF in (1), requires mapping an uniform random distribution ($0 \leq x \leq 1$) to cosine angular PDF, involves a simple change of variables,

$$x = \frac{\int_0^\theta f(\theta)\mathrm{d}\theta}{\int_0^{\pi/2} f(\theta)\mathrm{d}\theta} = \frac{\int_0^\theta \cos\theta \mathrm{d}\theta}{1} = \sin\theta$$

therefore

$$\theta = \sin^{-1} x$$

Simulating $\cos(x)$ with $x \in [-\pi/2, \pi/2]$ would provide erroneous results.

Algorithm 2 A Simplified Method to Generate Correlated Rayleigh Envelopes Using Multivariate Normal Random Numbers

Input: R, A, mc-iteration
Output: $\mathbf{h}, P_{out}$
Monte Carlo
for mc = 1 to iteration **do**
  $\mathbf{a} = \mathrm{mvnrnd}\left((0)^{1XN}, R^{NXN}\right)$
  $\mathbf{b} = \mathrm{mvnrnd}\left((0)^{1XN}, R^{NXN}\right)\mathrm{j}$
  $\mathbf{h} = (\mathbf{a} + \mathbf{b})/\sqrt{(2)}$
end for
return h

Note: mvnrnd is the Multivariate normal random number generator which needs a 1XN zero vector and NXN covariance vector as inputs and provides 1XN complex outputs with correlated Rayleigh envelopes. It is readily available in mvnrnd tool in MATLAB and numpy.random.multivariate_normal in python.

ACKNOWLEDGMENT

(Renjith Ravindran Unnithan Jalaja and Vetrivel Chelian Thirumavalavan contributed equally to this work.) The authors would like to thank the management of Thiagarajar College of Engineering, Madurai, for their constant support.

REFERENCES

[1] C. Huang, S. Hu, G. C. Alexandropoulos, A. Zappone, C. Yuen, R. Zhang, M. D. Renzo, and M. Debbah, "Holographic MIMO surfaces for 6G wireless networks: Opportunities, challenges, and trends," *IEEE Wireless Commun.*, vol. 27, no. 5, pp. 118–125, Jul. 2020.
[2] A. Pizzo, T. L. Marzetta, and L. Sanguinetti, "Spatially-stationary model for holographic MIMO small-scale fading," *IEEE J. Sel. Areas Commun.*, vol. 38, no. 9, pp. 1964–1979, Sep. 2020.
[3] N. Rajatheva *et al.*, "White paper on broadband connectivity in 6G," 2020, *arXiv:2004.14247*. [Online]. Available: http://arxiv.org/abs/2004.14247
[4] S. Dang, O. Amin, B. Shihada, and M.-S. Alouini, "What should 6G be?" *Nature Electron.*, vol. 3, no. 1, pp. 20–29, Jan. 2020.
[5] F. Tariq, M. R. A. Khandaker, K.-K. Wong, M. A. Imran, M. Bennis, and M. Debbah, "A speculative study on 6G," *IEEE Wireless Commun.*, vol. 27, no. 4, pp. 118–125, Aug. 2020.
[6] L. Zhang, X. Q. Chen, S. Liu, Q. Zhang, J. Zhao, J. Y. Dai, G. D. Bai, X. Wan, Q. Cheng, G. Castaldi, and V. Galdi, "Space-time-coding digital metasurfaces," *Nature Commun.*, vol. 9, no. 1, p. 4334, 2018.
[7] J. C. B. Garcia, A. Sibille, and M. Kamoun, "Reconfigurable intelligent surfaces: Bridging the gap between scattering and reflection," *IEEE J. Sel. Areas Commun.*, vol. 38, no. 11, pp. 2538–2547, Nov. 2020.
[8] S. Buzzi, C.-L. I, T. E. Klein, H. V. Poor, C. Yang, and A. Zappone, "A survey of energy-efficient techniques for 5G networks and challenges ahead," *IEEE J. Sel. Areas Commun.*, vol. 34, no. 4, pp. 697–709, Apr. 2016.
[9] C. Huang, A. Zappone, G. C. Alexandropoulos, M. Debbah, and C. Yuen, "Reconfigurable intelligent surfaces for energy efficiency in wireless communication," *IEEE Trans. Wireless Commun.*, vol. 18, no. 8, pp. 4157–4170, Aug. 2019.
[10] C. Pan, H. Ren, K. Wang, M. Elkashlan, A. Nallanathan, J. Wang, and L. Hanzo, "Intelligent reflecting surface aided MIMO broadcasting for simultaneous wireless information and power transfer," *IEEE J. Sel. Areas Commun.*, vol. 38, no. 8, pp. 1719–1734, Aug. 2020.
[11] T. Bai, C. Pan, H. Ren, Y. Deng, M. Elkashlan, and A. Nallanathan, "Resource allocation for intelligent reflecting surface aided wireless powered mobile edge computing in OFDM systems," 2020, *arXiv:2003.05511*. [Online]. Available: http://arxiv.org/abs/2003.05511
[12] E. Basar, "Transmission through large intelligent surfaces: A new frontier in wireless communications," in *Proc. Eur. Conf. Netw. Commun. (EuCNC)*, Jun. 2019, pp. 112–117.
[13] E. Basar, "Reconfigurable intelligent surface-based index modulation: A new beyond MIMO paradigm for 6G," *IEEE Trans. Commun.*, vol. 68, no. 5, pp. 3187–3196, May 2020.
[14] O. Yurduseven, S. D. Assimonis, and M. Matthaiou, "Intelligent reflecting surfaces with spatial modulation: An electromagnetic perspective," *IEEE Open J. Commun. Soc.*, vol. 1, pp. 1256–1266, 2020.
[15] I. Yildirim, F. Kilinc, E. Basar, and G. C. Alexandropoulos, "Hybrid RIS-empowered reflection and decode-and-forward relaying for coverage extension," *IEEE Commun. Lett.*, early access, Jan. 26, 2021, doi: 10.1109/LCOMM.2021.3054819.
[16] X. Ying, U. Demirhan, and A. Alkhateeb, "Relay aided intelligent reconfigurable surfaces: Achieving the potential without so many antennas," 2020, *arXiv:2006.06644*. [Online]. Available: https://arxiv.org/abs/2006.06644
[17] A.-A.-A. Boulogeorgos and A. Alexiou, "How much do hardware imperfections affect the performance of reconfigurable intelligent surface-assisted systems?" *IEEE Open J. Commun. Soc.*, vol. 1, pp. 1185–1195, 2020.
[18] E. Bjornson, O. Ozdogan, and E. G. Larsson, "Intelligent reflecting surface versus decode-and-forward: How large surfaces are needed to beat relaying?" *IEEE Wireless Commun. Lett.*, vol. 9, no. 2, pp. 244–248, Feb. 2020.
[19] M. Di Renzo, K. Ntontin, J. Song, F. H. Danufane, X. Qian, F. Lazarakis, J. De Rosny, D.-T. Phan-Huy, O. Simeone, R. Zhang, M. Debbah, G. Lerosey, M. Fink, S. Tretyakov, and S. Shamai, "Reconfigurable intelligent surfaces vs. relaying: Differences, similarities, and performance comparison," *IEEE Open J. Commun. Soc.*, vol. 1, pp. 798–807, 2020.

[20] I. Chatzigeorgiou, "The impact of 5G channel models on the performance of intelligent reflecting surfaces and decode-and-forward relaying," in *Proc. IEEE 31st Annu. Int. Symp. Pers., Indoor Mobile Radio Commun.*, Aug. 2020, pp. 1–4.

[21] L. Yang, Y. Yang, M. O. Hasna, and M.-S. Alouini, "Coverage, probability of SNR gain, and DOR analysis of RIS-aided communication systems," *IEEE Wireless Commun. Lett.*, vol. 9, no. 8, pp. 1268–1272, Aug. 2020.

[22] M. T. Ivrlac and J. A. Nossek, "Quantifying diversity and correlation in Rayleigh fading MIMO communication systems," in *Proc. 3rd IEEE Int. Symp. Signal Process. Inf. Technol.*, Dec. 2003, pp. 158–161.

[23] E. Jorswieck and H. Boche, *Majorization and Matrix-Monotone Functions in Wireless Communications*, vol. 3. Boston, MA, USA: Now, 2007.

[24] E. Bjornson and L. Sanguinetti, "Rayleigh fading modeling and channel hardening for reconfigurable intelligent surfaces," *IEEE Wireless Commun. Lett.*, early access, Dec. 21, 2020, doi: 10.1109/LWC.2020.3046107.

[25] M. Patzold, *Mobile Fading Channels: Modelling, Analysis and Simulation*. Hoboken, NJ, USA: Wiley, 2001.

[26] E. Björnson, Ö. Özdogan, and E. G. Larsson, "Reconfigurable intelligent surfaces: Three myths and two critical questions," *IEEE Commun. Mag.*, vol. 58, no. 12, pp. 90–96, Dec. 2020.

[27] E. Bjornson and L. Sanguinetti, "Power scaling laws and near-field behaviors of massive MIMO and intelligent reflecting surfaces," *IEEE Open J. Commun. Soc.*, vol. 1, pp. 1306–1324, 2020.

[28] E. J. Black, "Holographic beam forming and MIMO," Pivotal Commware, White Paper, Dec. 2017, pp. 6–8.

[29] H. Lu, Y. Zeng, S. Jin, and R. Zhang, "Enabling panoramic full-angle reflection via aerial intelligent reflecting surface," in *Proc. IEEE Int. Conf. Commun. Workshops (ICC Workshops)*, Jun. 2020, pp. 1–6.

[30] *3rd Generation Partnership Project; Technical Specification Group Radio Access Network; Evolved Universal Terrestrial Radio Access (E-Utra); User Equipment (UE) Conformance Specification Radio Transmission and Reception*, document 36.521-3, 2008.

[31] B. Natarajan, C. R. Nassar, and V. Chandrasekhar, "Generation of correlated Rayleigh fading envelopes for spread spectrum applications," *IEEE Commun. Lett.*, vol. 4, no. 1, pp. 9–11, Jan. 2000.

[32] M. Fisz and R. Bartoszyński, *Probability Theory and Mathematical Statistics*, vol. 3. Hoboken, NJ, USA: Wiley, 2018.

[33] S. András and Á. Baricz, "Properties of the probability density function of the non-central chi-squared distribution," *J. Math. Anal. Appl.*, vol. 346, no. 2, pp. 395–402, Oct. 2008.

[34] A. Nuttall, "Some integrals involving the Q_M function (Corresp.)," *IEEE Trans. Inf. Theory*, vol. IT-21, no. 1, pp. 95–96, Jan. 1975.

[35] A. Annamalai, C. Tellambura, and J. Matyjas, "A new twist on the generalized marcum Q-function Q_M(a, b) with fractional-order M and its applications," in *Proc. 6th IEEE Consum. Commun. Netw. Conf.*, Jan. 2009, pp. 1–5.

[36] S. Kotz and R. Srinivasan, "Distribution of product and quotient of Bessel function variates," *Ann. Inst. Stat. Math.*, vol. 21, no. 1, pp. 201–210, 1969.

[37] N. L. Johnson, S. Kotz, and N. Balakrishnan, *Continuous Univariate Distributions*, vol. 1. Boston, MA, USA: Houghton Mifflin, 1970.

[38] T. Mao, Q. Wang, Z. Wang, and S. Chen, "Novel index modulation techniques: A survey," *IEEE Commun. Surveys Tuts.*, vol. 21, no. 1, pp. 315–348, 1st Quart., 2019.

[39] R. Y. Mesleh, H. Haas, S. Sinanovic, C. W. Ahn, and S. Yun, "Spatial modulation," *IEEE Trans. Veh. Technol.*, vol. 57, no. 4, pp. 2228–2241, Jul. 2008.

[40] *Fundamentals of RF and Microwave Noise Figure Measurements*, Santa Rosa, CA, USA: Keysight Technologies, 2014.

RENJITH RAVINDRAN UNNITHAN JALAJA (Member, IEEE) received the master's degree from the Jayaram College of Engineering and Technology, Tiruchirappalli. He is currently pursuing the Ph.D. degree with the Signal Processing Laboratory, Thiagarajar College of Engineering, Madurai, under the AICTE-QIP Scheme. His research interests include investigating energy harvesting and SWIPT systems and has keen interest in index modulation.

VETRIVEL CHELIAN THIRUMAVALAVAN (Graduate Student Member, IEEE) received the master's degree in engineering from the College of Engineering, Guindy, in 2017. He is currently pursuing the Ph.D. degree in wireless communication with the Thiagarajar College of Engineering, Madurai. His research interests include array signal processing, intelligent reflecting surfaces, and holographic radios.

PERIAKARUPAN GURUSAMY SIVABALAN VELMURUGAN (Member, IEEE) received the Ph.D. degree in information and communication from Anna University, in 2015. He is currently an Assistant Professor with the Department of Electronics and Communication, Thiagarajar College of Engineering, Madurai. His research interests include physical layer network coding, co-operative communications, convex optimization, and USRP based analytics.

SUNDARRAJAN JAYARAMAN THIRUVENGADAM (Senior Member, IEEE) received the B.E. degree in electronics and communication engineering from the Thiagarajar College of Engineering, Madurai, India, in 1991, the M.E. degree in applied electronics from College of Engineering, Guindy, Chennai, India, in 1994, and the Ph.D. degree from Madurai Kamaraj University, Madurai, in 2005. From January 2008 to December 2008, he was a Visiting Associate Professor with the Department of Electrical Engineering, Stanford University, Stanford, CA, USA, under a Postdoctoral Fellowship, by the Department of Science and Technology, Government of India. He is currently a Professor and Dean (Academics) with the Department of Electronics and Communication Engineering, Thiagarajar College of Engineering. His research interests include statistical signal processing and MIMO wireless communications.